Vacancy-defective spinel $NiCo_2O_4$ enables high-valent Ni/Co species and adsorbate binding for the electrocatalytic upcycling of polybutylene succinate plastics

Jiahui Xian[1,2], Ziyu Mi[1,2], Panyawut Tonanon[1], Xun Cao[2], Richard D. Webster[1] and Wan Ru Leow[1,2]*

[1]School of Chemistry, Chemical Engineering and Biotechnology, Nanyang Technological University; 21 Nanyang Link, Nanyang Technological University, Singapore 637371, Republic of Singapore

[2]Institute of Sustainability for Chemicals Energy and Environment (ISCE[2]), Agency for Science, Technology and Research (A*STAR); 1 Pesek Road Jurong Island, Singapore 627833, Republic of Singapore

*Corresponding authors. Email: wanru.leow@ntu.edu.sg

Experimental section

Catalyst preparation

$NiCo_2O_4$ array electrocatalyst was grown directly on the Ni foam via a hydrothermal method followed by annealing procedure. Specifically, 1 mmol of $Ni(NO_3)_2 \cdot 6H_2O$, 2 mmol of $Co(NO_3)_2 \cdot 6H_2O$, 10 mmol of urea and 5 mmol NH_4F were dissolved in 40 mL deionized water under constant stirring to form a uniform solution. Then, the mixture solution was transferred into a Teflon-lined autoclave and a piece of pretreated Ni foam (3×4 cm^2, 1.5 mm thickness) was immersed in above solution. The stainless steel autoclave was sealed and heated at 120℃ for 6 h in an oven. After cooling to room temperature, the resulting precursor was thoroughly washed with deionized water and ethanol and then dried at 60°C. $NiCo_2O_4$ array electrocatalyst was obtained by calcination of the as-prepared precursor in air at 450°C for 3 h with a ramp rate of 2℃ min^{-1}. For comparison, the NiO, $NiFe_2O_4$, NiCuO, NiZnO and Co_3O_4 electrodes were prepared using the same method, with the total metal ion concentration kept constant while varying the metal ion type.

Materials characterization

X-ray diffraction (XRD) was performed on Bruker® D8 ADVANCE with Cu Kα source. Scanning electron microscopy (SEM) images were obtained on a Hitachi SU8220 FESEM at an accelerating voltage of 5 kV. Energy-dispersive X-ray (EDX) spectroscopy was recorded in an on-board AEMTEK® Octane Elite EDS System, with an accelerating voltage of 20 kV. Transmission electron microscopy (TEM) images were obtained on TEM JEOL 2100F. X-ray photoelectron spectroscopy (XPS) was measured on a PHI Quantum 2000 XPS system, with the C 1*s* peak at 284.8 eV as the energy standard. Raman spectroscopic data was obtained using a Renishaw inVia Raman Microscope with a 532 nm laser. ^1H nuclear magnetic resonance (^1H NMR) spectra were recorded on Bruker Ascend^{TM} 400 (400 MHz). Electron paramagnetic resonance (EPR) spectra were recorded on a continuous-wave X-band Bruker ELEXSYS E500 EPR spectrometer. The center field is 3490G, and sweep width 200G, with microwave frequency 9.79 GHz.

Electrochemical Measurements

The electrochemical measurements were performed using a standard three-electrode cell (purchased from Tianjin Aida) connected to an electrochemical workstation (Metrohm Autolab potentiostat PGSTAT204). The as-synthesized catalyst on NF was employed as the working electrode (effective area 1 cm^2), with a platinum plate as the counter electrode and an Ag/AgCl (saturated KCl) electrode as the reference electrode. Electrochemical BDO oxidation reaction (BOR) was conducted in an H-type cell using 1.0 M NaOH solution with 0.1 M BDO as the anolyte and 1.0 M NaOH solution as the catholyte, separated by Nafion® 117 membrane (size 2.5 cm by 2.5 cm, thickness 0.18mm). All data reported were recorded without iR compensation, and all the potentials were referenced to the reversible hydrogen electrode (RHE) using the following equation: $E_{RHE} = E_{Ag/AgCl} + 0.0591 \times pH + 0.197$. The cyclic voltammetry (CV) and linear sweep voltammetry (LSV) curves were measured at a scan rate of 10 mV s^{-1} without iR-correction unless otherwise noted. In situ electrochemical impedance spectroscopy (EIS) tests were tested at the potentials of 1.05 to 1.60 V vs. RHE with a frequency range from 10^{-1} to 10^5 Hz with an alternating-current amplitude of 10 mV. Electrochemical double-layer capacitance (C_{dl}) measurement was carried out by CV method with different scan rates in the non-Faradaic region. The C_{dl} value was obtained from the slopes of the current density–scan rate plots.

The electrocatalytic upcycling of PBS plastic was performed using PBS hydrolysate as the electrolyte. Before electrocatalysis, PBS plastic was hydrolyzed in an alkaline solution to obtain the PBS hydrolysate. Briefly, 5 g of PBS plastic was soaked in 60 mL 2.0 M NaOH solution within a 100 mL Teflon-lined autoclave, which was sealed and maintained at 120℃ for 10 h. After cooling to room temperature, the resulting clear aqueous solution was denoted as PBS hydrolysate and employed for further PBS upcycling experiments. The co-electrolysis system by coupling BOR with NO_2^-RR was constructed in a membrane electrode assembly (MEA) electrolyzer with $NiCo_2O_4$ anode and OD-Cu cathode. The paired BOR|| NO_2^-RR system was used for PBS hydrolysate recovery, with the diluted PBS hydrolysate as the anolyte and 1.0 M NaOH containing 0.15 M NO_2^- as the catholyte. Both electrolytes were circulated at a flow rate of 30 mL min^{-1}. The electrocatalytic performance of BOR and NO_2^-RR was

evaluated simultaneously.

Product analysis

The post-reaction electrolyte was collected and analyzed by ^{1}H nuclear magnetic resonance (^{1}H NMR, Bruker AV400) with water suppression. For anolyte analysis, a mixture of 350 μL electrolyte, 100 μL D_2O, and 50 μL DMSO aqueous solution (50 mM) as an internal standard was prepared. For cathodic NH_3 analysis, 350 μL of electrolyte (adjusted to pH 2.0) was mixed with 100 μL DMSO-*d*6 and 50 μL maleic acid aqueous solution (50 mM) as an internal standard. Both samples were then analyzed by ^{1}H NMR.

The Faradaic efficiency, selectivity, conversion and yield for liquid product are calculated using the following equations:

$$\text{Faradaic efficiency (\%)} = (N \times F \times C_x \times V) / Q \times 100\%$$

$$\text{Selectivity (\%)} = (C_x \times V) / n_c \times 100\%$$

$$\text{Conversion (\%)} = n_c / n_i \times 100\%$$

$$\text{Yield (\%)} = \text{Conversion} \times \text{Selectivity}$$

where N is the number of electron transfer to generated product, F is the Faraday constant (96485 C mol^{-1}), C_x is the concentration of liquid products after the electrosynthesis reaction, V is the volume of the electrolyte, Q is the total charge during the electrosynthesis process, n_c is the mole amount of consumed feedstock, n_i is the mole amount of initial feedstock.

In situ spectroelectrochemical measurements

In situ ATR-SEIRAS was conducted on a PerkinElmer Frontier FT-IR spectrometer equipped with a mercury cadmium telluride (MCT) detector, using a commercial electrochemical cell with 1.0 M NaOH containing 0.1 M BDO electrolyte. An ultrathin Au film was chemically deposited on the reflective plane of a Si ATR prism, onto which the $NiCo_2O_4$ electrocatalyst was drop-cast and dried. Prior to each measurement, the background spectrum without applied potential was acquired at electrolyte condition. Each reported spectrum was obtained by subtracting the corresponding background. During in situ measurements, the electrode was maintained at each applied potential for 300 s to reach a steady state before spectrum collection. In situ spectra were recorded at potentials ranging from OCP to 1.60 V vs. RHE, with 50 scans

averaged at a resolution of 4 cm^{-1}.

In situ electrochemical Raman measurements were conducted using a confocal Raman microscope equipped with 532 nm excitation laser and a spectra-electrochemical quartz cell. $NiCo_2O_4$ deposited on carbon paper served as the working electrode, with an Ag/AgCl electrode as the reference and a Pt wire as the counter electrode. In situ Raman spectra under different electrochemical conditions were collected in 1.0 M NaOH, both with and without 0.1 M BDO in the electrolyte, with a 300 s hold at each potential.

Density functional theory (DFT) calculations

All the calculations are performed in the framework of the density functional theory (DFT) with the projector augmented plane-wave method, as implemented in the Vienna ab initio simulation package.[1] The generalzied gradient approximation proposed by Perdew, Burke, and Ernzerhof is selected for the exchange-correlation potential.[2] The cut-off energy for plane wave is set to 450 eV. The energy criterion is set to 10^{-5} eV in iterative solution of the Kohn-Sham equation. A vacuum layer of 15 Å is added perpendicular to the sheet to avoid artificial interaction between periodic images. The Brillouin zone integration is performed using a 2x2x1 k-mesh. During structural optimization, all the structures are relaxed until the residual forces on the atoms have declined to less than 0.05 eV/Å, while the bottom 2 layer was fixed in its main body position.

The adsorption energy (E_{ads}) was calculated using the formula as follows:

$E_{ads} = E_{total} - E_{substrate} - E_{adsorbate}$

where E_{total} is the energy of *OH or BDO adsorbed respectively on the $NiCo_2O_4$ and Co_3O_4 surface, $E_{substate}$ is the energy of catalyst surface, and $E_{adsorbate}$ is the energy of *OH or BDO molecules.

Techno-economic Analysis (TEA)

To assess the economic feasibility of paired BOR||NO_2^-RR system using PBS waste plastic and nitrite, a techno-economic analysis (TEA) was performed based on recently reported models.[3, 9-11] The costs are categorized into three main areas: raw material cost, capital cost and operation cost. The capital costs are primarily attributed to the costs of the electrolyzer, catalyst,

hydrolyzer equipment and separation equipment. The operating costs are dominated by electricity cost, and on this basis, the separation cost, factory operation cost and other costs are calculated. Profits are generated from the sale of the products obtained at the anode (SA and $NaHCO_3$) and cathode (NH_3). The TEA is conducted based on the optimized operational parameters of the paired MEA electrolyzer. The specific assumptions used in TEA are listed as follows:

1. The electrolyzer served a critical role in the electroreforming of PBS plastics, with an estimated cost of \$10,000 per m^2. The electrolyzer is anticipated to have a lifespan of a decade, operating 350 days annually.
2. The catalyst cost is assumed to be 5% of the electrolyzer cost.
3. The capital costs of hydrolyzer equipment costs are assumed to be 50% of PBS feedstock cost.
4. The capital costs of separation equipment are set at 10% of the electrolyzer's cost.
5. The cost of Balance of Plant is calculated as 58% of the electrolyzer's cost.
6. The plant operates with an 80% capacity factor, operating for 19.2 hours daily.
7. Operation and maintenance costs are set at 10% of capital costs.
8. The cost of renewable electricity is taken to be \$0.1 per kWh^{-1}. The electricity costs comprise three components: electrolysis, hydrolysis, and separation processes.
9. The separation costs are 20 % of electricity costs.
10. The hydrolysis costs are 10 % of electricity costs.
11. The processing capacity of the plant is 1 ton of PBS waste plastic per day.
12. The input raw materials include PBS, NaOH, $NaNO_2$, HCl, and water, while the output products include SA, $NaHCO_3$ and NH_3. The prices of chemicals are summarized in Table S5.
13. During electrosynthesis, the Faradaic efficiency of SA is assumed to be 90%. The yield of $NaHCO_3$ is assumed to be 60%. The Faradaic efficiency of NH_3 at the cathode (for BOR||NO_2^-RR model) is estimated at 90%.
14. The operation was carried out at 1.5 V, with the current density of 400 mA cm^{-2}.

The detailed calculations of each component were listed as follows:

Raw material costs:

The materials required are 1 ton of PBS, 2.67 tons of NaOH, 1.24 tons of $NaNO_2$, 67 tons of water, and 4 tons of concentrated HCl.

$$Raw\ material\ costs = \frac{1 \times 390 + 2.67 \times 422 + 1.24 \times 571 + 67 \times 0.22 + 4 \times 12.7}{0.94}$$

$$= \$2436.5\ per\ ton_{SA}$$

Electricity costs:

We first calculate the total charge required to oxidize 1 ton of PBS per day:

$$Q = \frac{Mass\ of\ BDO\ converted \times F \times N}{Molar\ mass\ of\ BDO \times Faradaic\ efficinecy} = \frac{0.5 \times 10^6 \times 96485 \times 8}{90.12 \times 0.9}$$

$$= 4.76 \times 10^9 C$$

Where Q is the total charge, F is the Faraday's constant and N is the number of electrons transferred from BDO to SA.

We calculate the current (I) required to sustain this process:

$$I = \frac{Q}{Time\ in\ a\ day \times Capacity} = \frac{4.76 \times 10^9}{24 \times 3600 \times 0.8} = 6.88 \times 10^4 A$$

The power (P) required to sustain this process can be calculated.

$$P = 6.88 \times 10^4 \times 1.5 = 103.3\ kW$$

The energy use per day can be calculated as follows:

$$Energy\ use\ per\ day = 103.3 \times 24 \times 0.8 = 1983.4\ kWh$$

The electricity cost per day, normalized by the mass of SA produced, can be calculated as follows:

$$Electricity\ cost\ per\ day\ = \frac{Energy\ use\ per\ day \times Cost\ per\ kWh}{Mass\ of\ SA\ produced} = \frac{1983.4 \times 0.1}{0.94}$$

$$= \$211\ per\ ton_{SA}$$

Separation costs can be calculated as follows:

$$Separation\ costs = 211 \times 0.2 = \$42.2\ per\ ton_{SA}$$

Hydrolysis costs can be calculated as follows:

$$Hydrolysis\ costs = 211 \times 0.1 = \$21.1\ per\ ton_{SA}$$

Therefore, the electricity costs component can be calculated as follows:

$$Electricity\ costs = 211 + 42.2 + 21.1 = \$274.3\ per\ ton_{SA}$$

Capital costs:

We first calculate the electrolyzer cost:

$$Area\ of\ electrolyzer\ = \frac{I}{Current\ density} = \frac{6.88 \times 10^4 A}{0.4\ A\ cm^{-2}} = 17.2\ m^2$$

The electrolyzer cost can now be calculated as follows:

$$Cost\ of\ electrolyser = 17.2 \times 10000 = \$1.72 \times 10^5$$

The total catalyst cost is calculated as:

$$Cost\ of\ catalyst = 1.72 \times 10^5 \times 0.05 = \$8.6 \times 10^3$$

The capital costs associated with the separation equipment are calculated as:

$$Cost\ of\ separation\ equipment = 1.72 \times 10^5 \times 0.1 = \$1.72 \times 10^4$$

The capital costs of the hydrolyzer equipment are calculated as:

$$Cost\ of hydrolysis\ equipment = 390 \times 0.5 = \$195$$

Therefore, the capital costs component can be calculated as:

$$Capital\ costs$$
$$= \frac{electrolzer + catalyst + separation\ equipment + hydrolyzer\ equipment}{Lifetime\ of\ plant \times Mass\ of\ SA\ produced}$$
$$= \frac{1.72 \times 10^5 + 8.6 \times 10^3 + 1.72 \times 10^4 + 195}{10 \times 350 \times 0.94} = \$60.2\ per\ ton_{SA}$$

Operation costs:

$$Operation\ costs\ per\ day = 60.2 \times 0.1 = \$6.02\ per\ ton_{SA}$$

Maintenance cost:

$$Maintenance\ costs\ per\ day = 60.2 \times 0.1 = \$6.02\ per\ ton_{SA}$$

Balance of plant cost:

$$Balance\ of\ plant\ cost\ per\ day = \frac{1.72 \times 10^5 \times 0.58}{10 \times 350 \times 0.94} = \$30.3\ per\ ton_{SA}$$

Total costs:

$$Total\ costs = 2436.5 + 274.3 + 60.2 + 6.02 + 6.02 + 30.3 = \$2813.3\ per\ ton_{SA}$$

Output Chemicals value:

1 ton of PBS and 1.24 tons of $NaNO_2$ as raw material can produce 0.94 tons of SA, 3.36 tons of $NaHCO_3$ and 0.26 tons of NH_3. Therefore, the product value can be calculated as follows:

$$Total\ product\ value = 1957 \times 0.94 + 350 \times 3.36 + 750 \times 0.26 = \$3210.6$$

$$Value\ of\ SA\ t^{-1} = \frac{Total\ product\ value}{Mass\ of\ SA\ produced} = \frac{3210.6}{0.94} = \$3415.5\ per\ ton_{SA}$$

Total profits:

$$Total\ profit = Total\ product\ value - Total\ costs = 3415.5 - 2813.3$$
$$= \$602.2\ per\ ton_{SA}$$

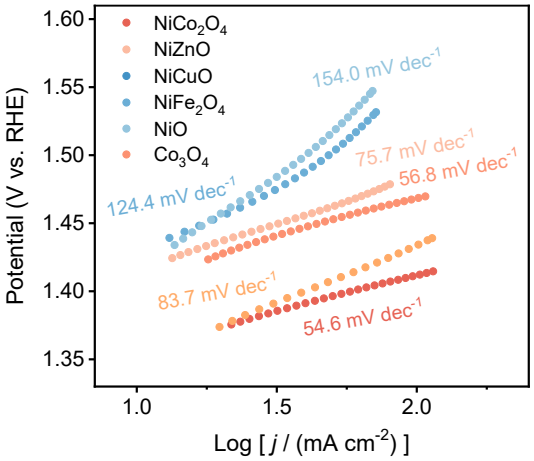

Fig. S1. Tafel slope of different electrocatalysts.

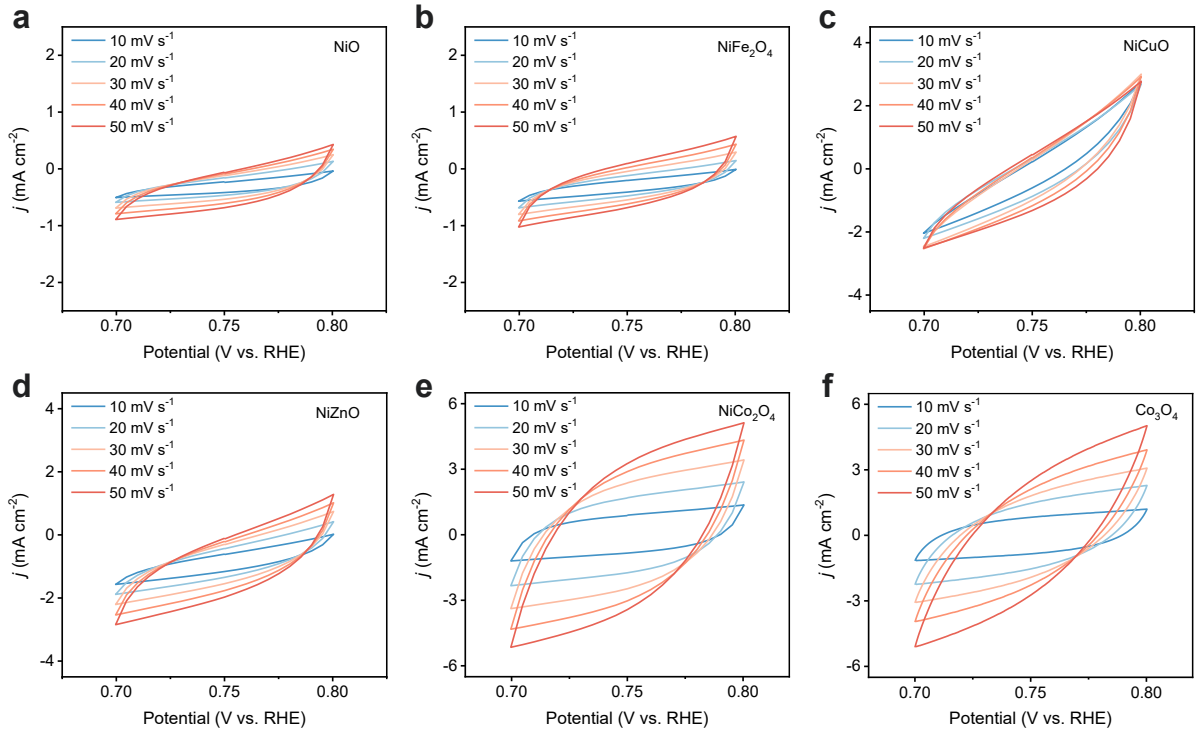

Fig. S2. CV curves in a non-Faradaic region at different scan rates with the (a) NiO, (b) $NiFe_2O_4$, (c) NiCuO, (d) NiZnO, (e) $NiCo_2O_4$ and (f) Co_3O_4 electrocatalysts.

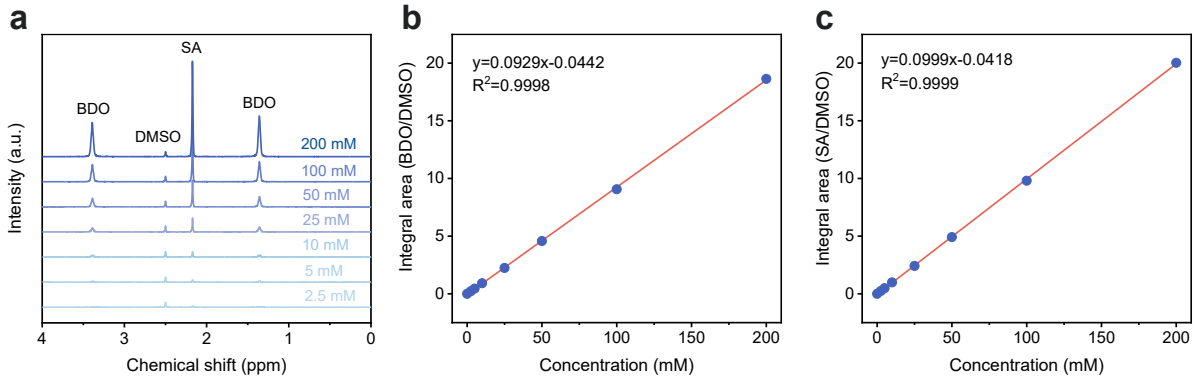

Fig. S3. (a) ^{1}H NMR spectra of BDO and SA of different concentrations in 1.0 M NaOH solution using dimethyl sulfoxide (DMSO) as an internal standard. The standard curve of NMR integral area (b) (BDO/DMSO) and (c) (SA/DMSO) plotted against a series of different concentration.

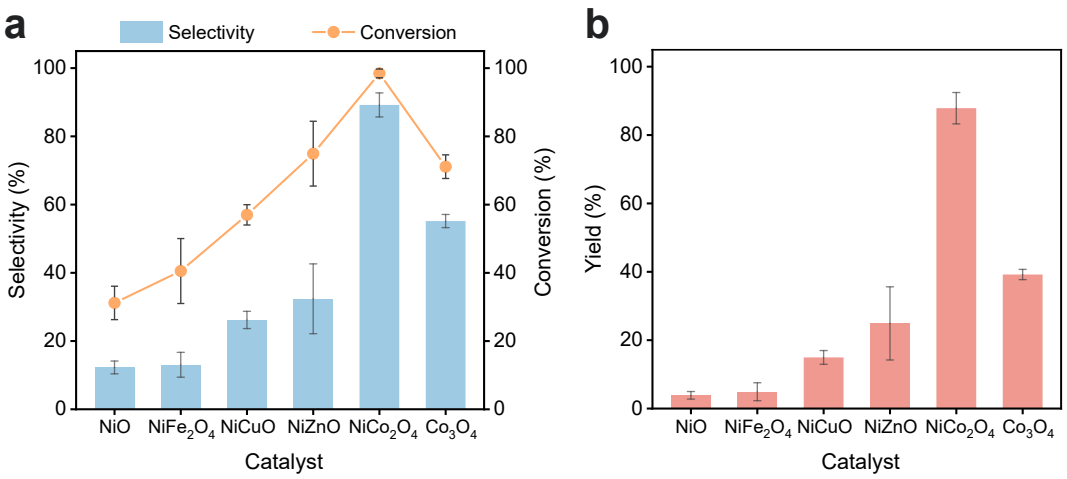

Fig. S4. (a) The selectivity of SA and the conversion of BDO, as well as (b) the yield of SA achieved with various electrocatalysts at 1.5 V vs. RHE.

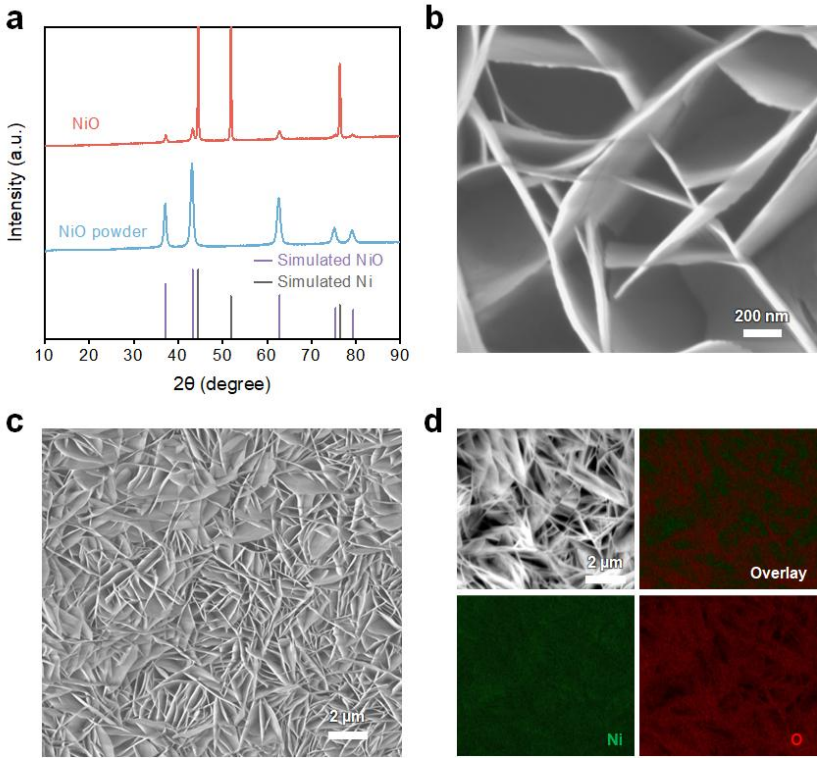

Fig. S5. (a) XRD patterns, (b-c) SEM images and (d) SEM-EDX elemental mapping of NiO electrocatalyst.

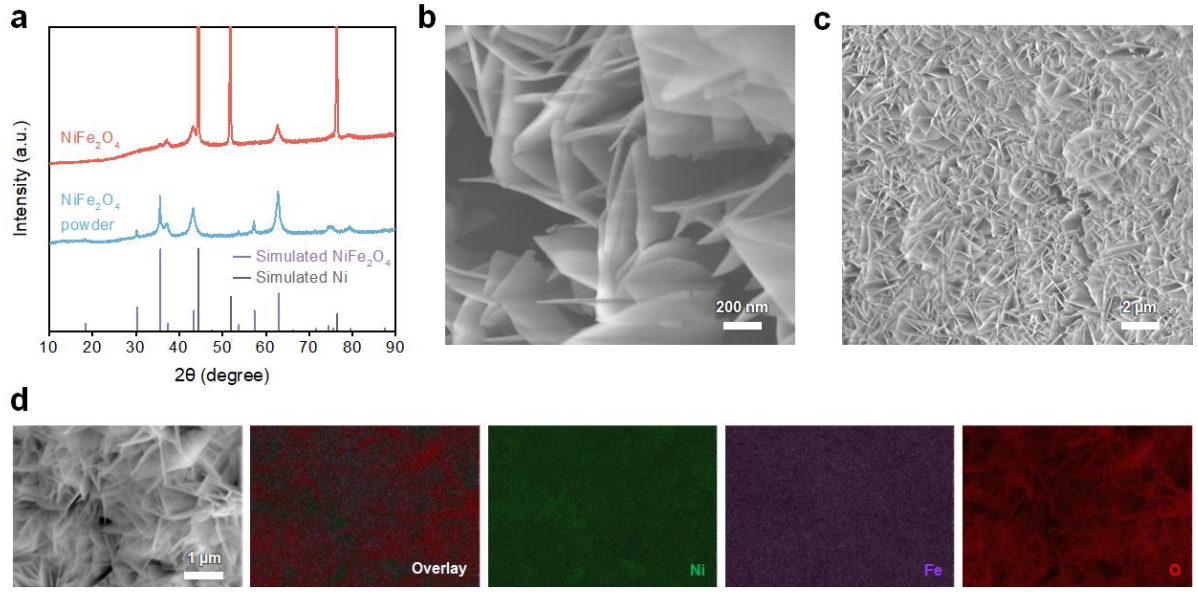

Fig. S6. (a) XRD patterns, (b-c) SEM images and (d) SEM-EDX elemental mapping of $NiFe_2O_4$ electrocatalyst.

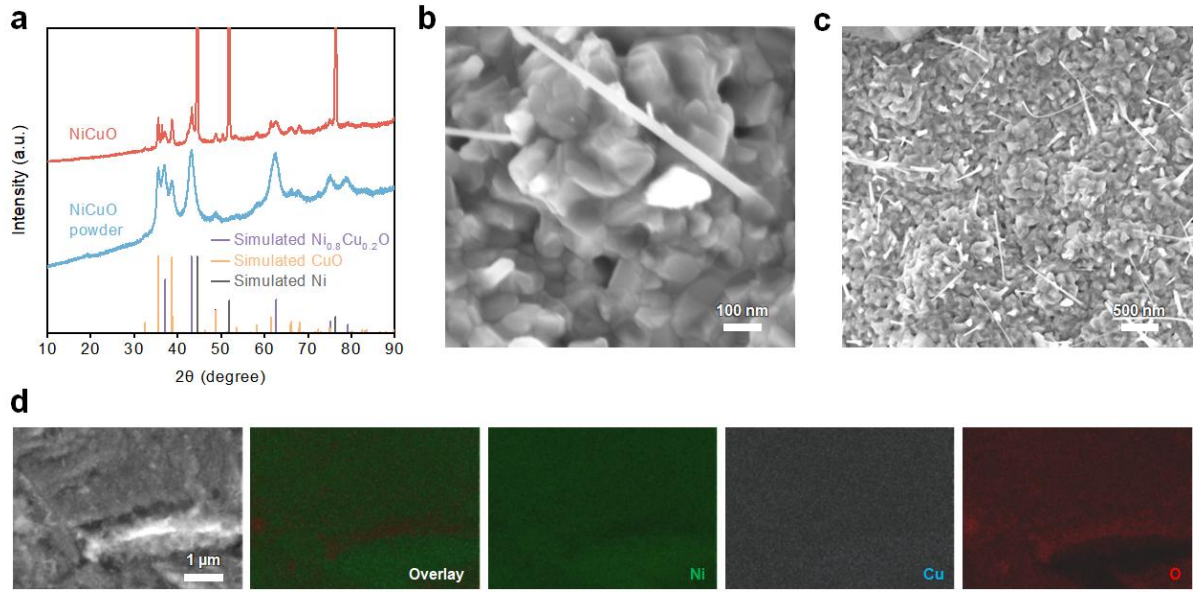

Fig. S7. (a) XRD patterns, (b-c) SEM images and (d) SEM-EDX elemental mapping of NiCuO electrocatalyst.

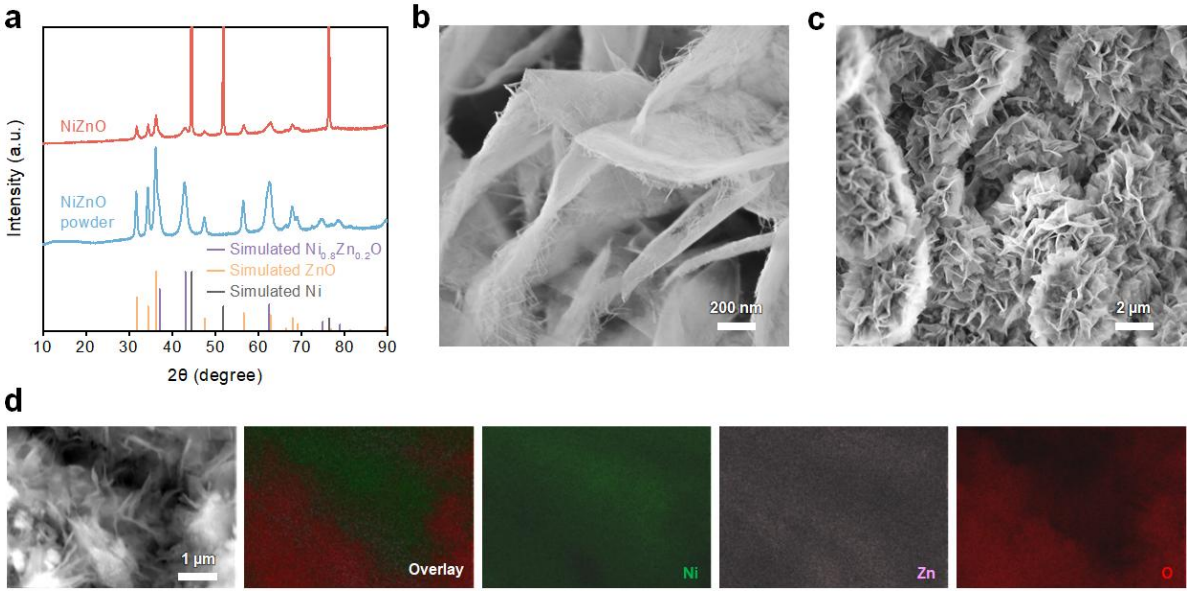

Fig. S8. (a) XRD patterns, (b-c) SEM images and (d) SEM-EDX elemental mapping of NiZnO electrocatalyst.

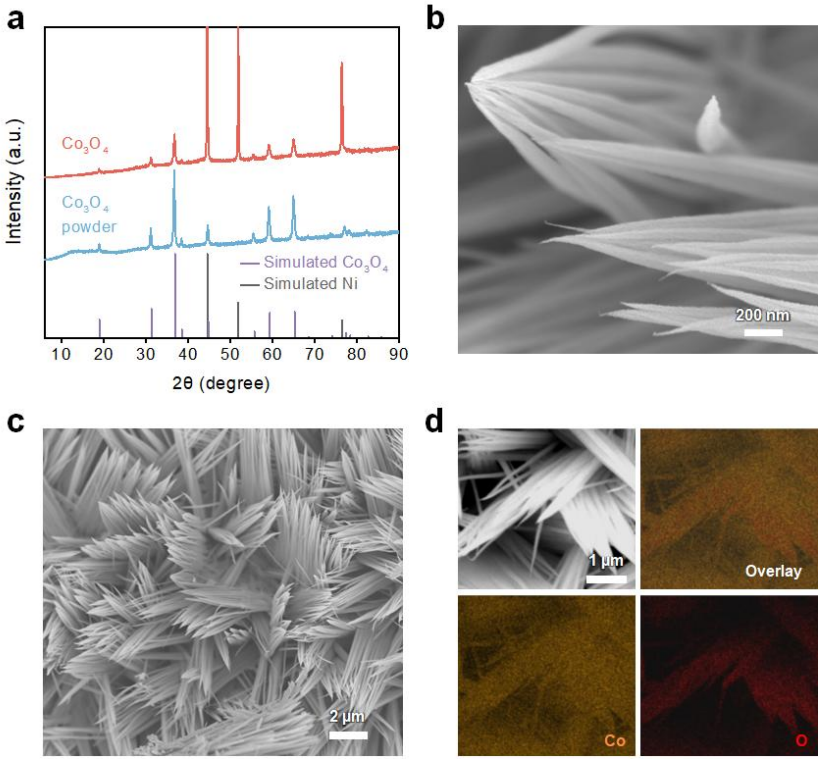

Fig. S9. (a) XRD patterns, (b-c) SEM images and (d) SEM-EDX elemental mapping of Co_3O_4 electrocatalyst.

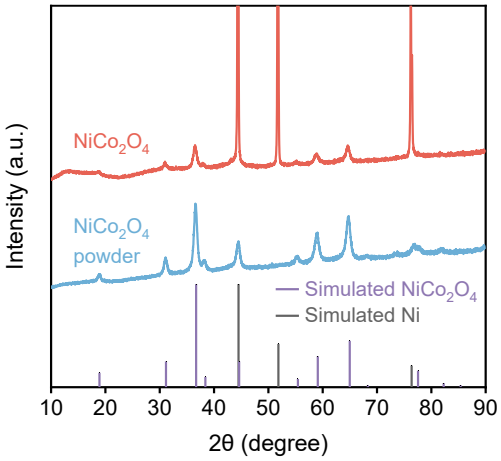

Fig. S10. XRD pattern of $NiCo_2O_4$ electrocatalyst.

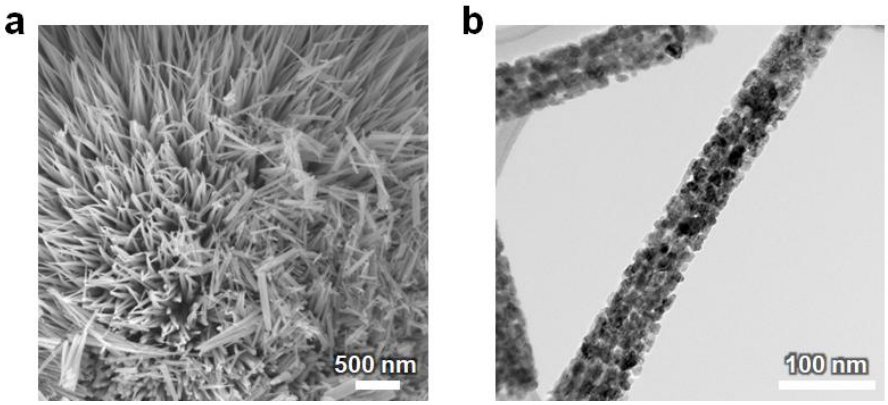

Fig. S11. (a) SEM and (b) TEM images of $NiCo_2O_4$ electrocatalyst.

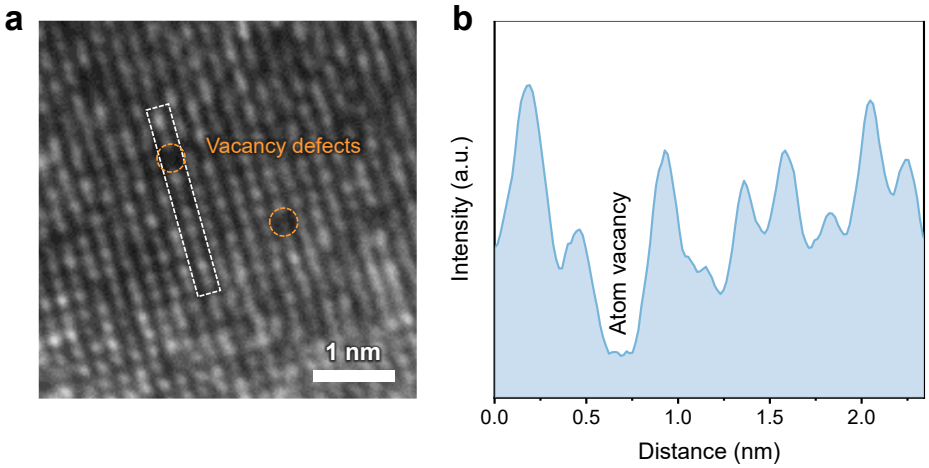

Fig. S12. (a) HRTEM image of $NiCo_2O_4$ electrocatalyst and (b) the integrated pixel intensity profile for the selected region.

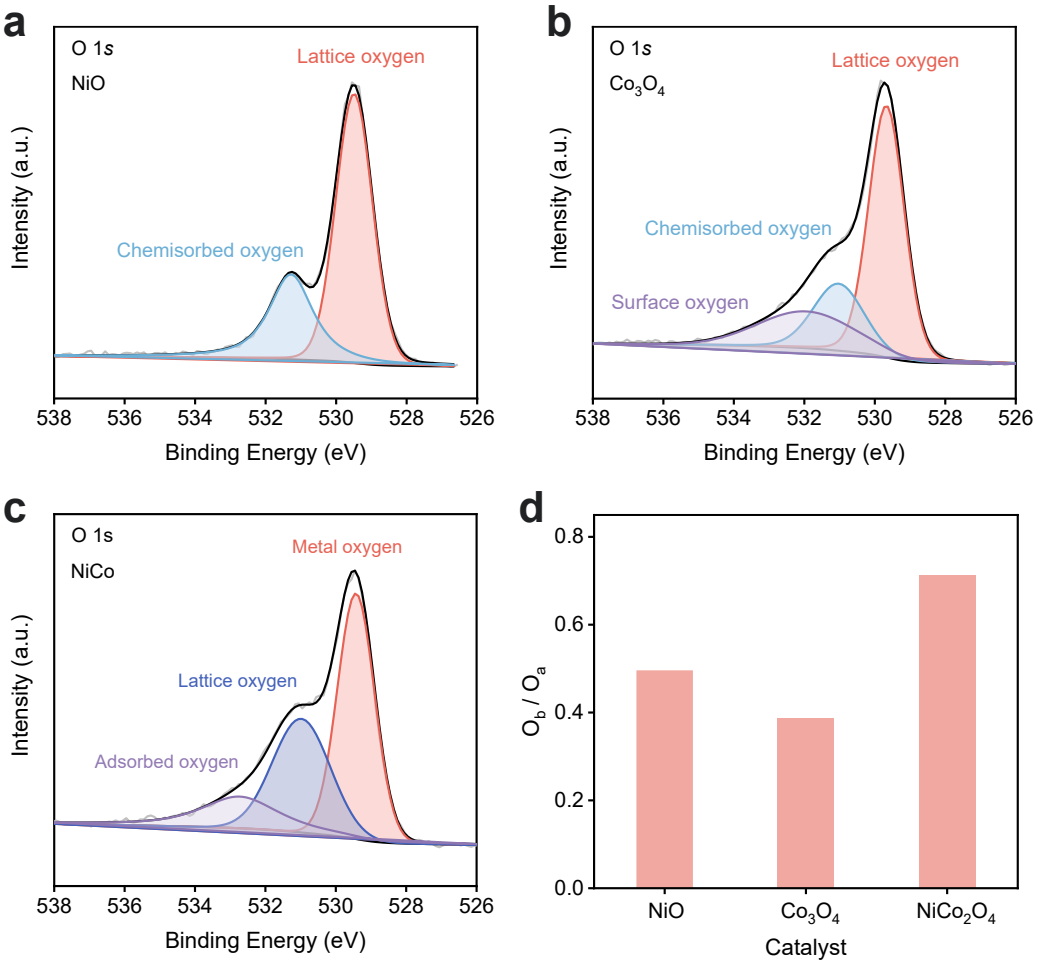

Fig. S13. High-resolution O 1*s* XPS spectra of (a) NiO, (b) Co_3O_4 and (c) $NiCo_2O_4$ electrocatalyst. (d) The lattice O/metal O (O_b/O_a) ratio obtained from O 1*s* XPS of the corresponding samples.

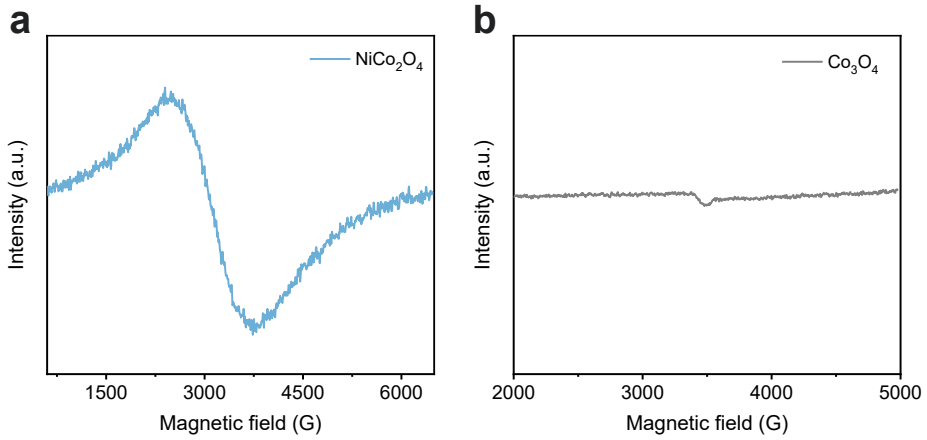

Fig. S14. EPR spectra of (a) $NiCo_2O_4$ and (b) Co_3O_4 electrocatalysts.

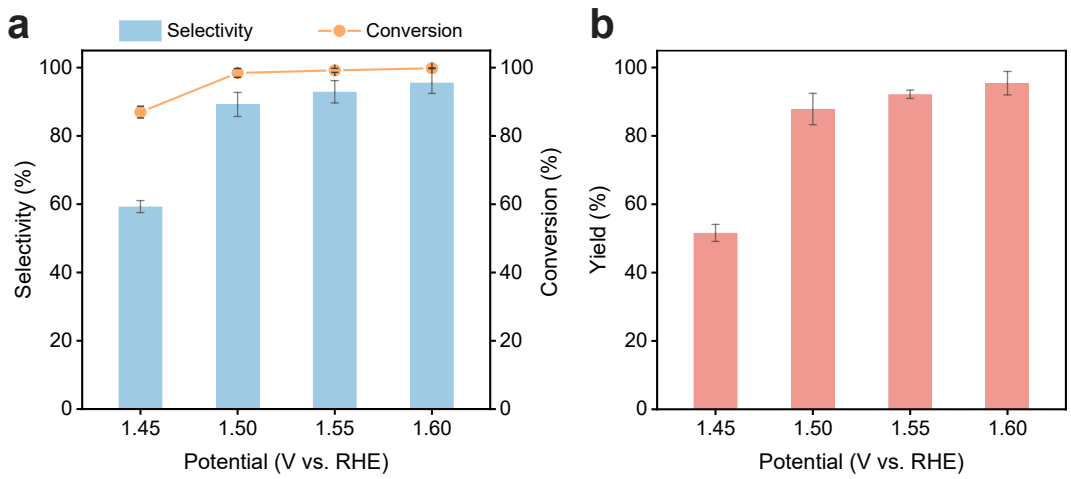

Fig. S15. (a) The selectivity of SA and the conversion of BDO, as well as (b) the yield of SA achieved over $NiCo_2O_4$ electrocatalyst at different applied potentials.

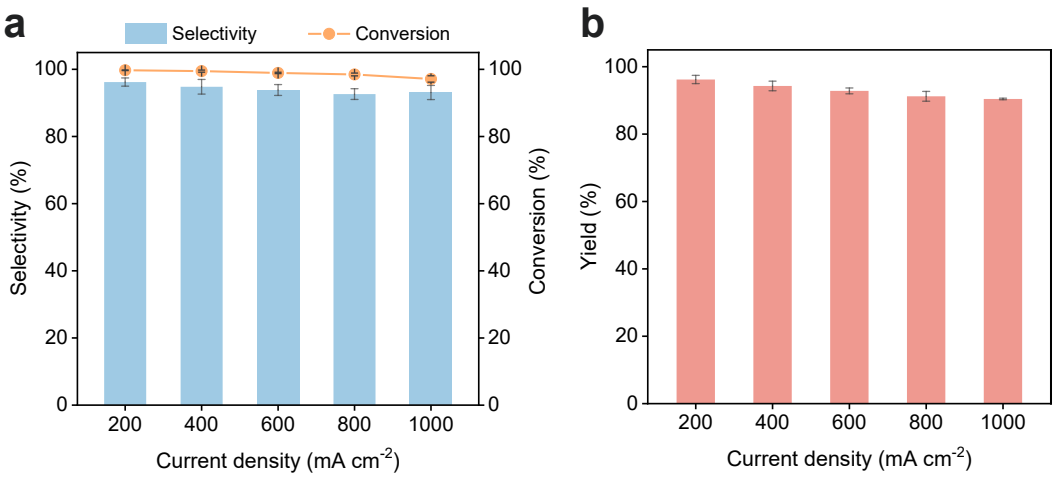

Fig. S16. (a) The selectivity of SA and the conversion of BDO, as well as (b) the yield of SA achieved over $NiCo_2O_4$ electrocatalyst at different current densities.

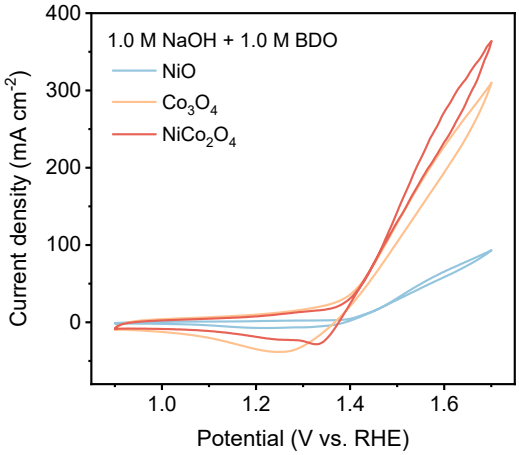

Fig. S17. CV curves of $NiCo_2O_4$, Co_3O_4 and NiO electrocatalysts in 1.0 M NaOH with 0.1 M BDO electrolyte.

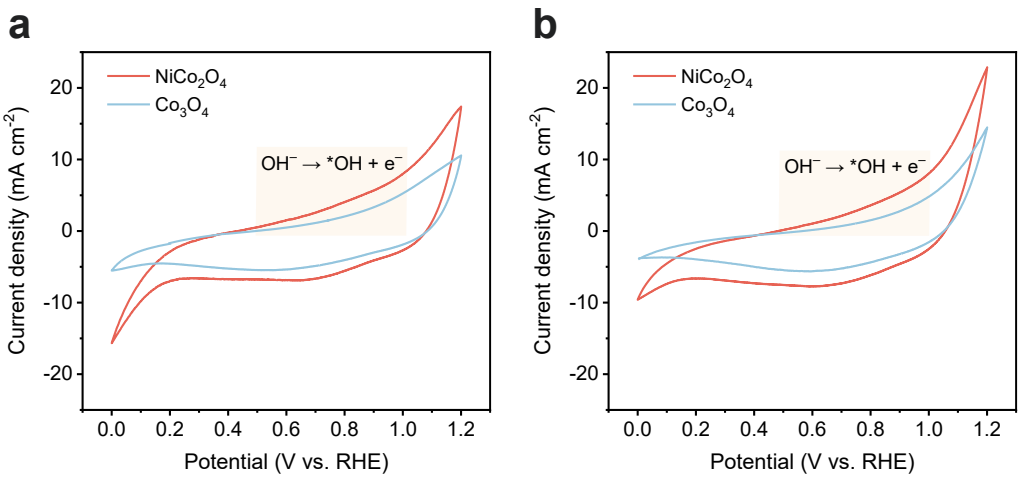

Fig. S18. CV curves of $NiCo_2O_4$ and Co_3O_4 electrocatalysts in Ar-saturated (a) 1.0 M NaOH and (b) 1.0 M NaOH with 0.1 M BDO electrolyte.

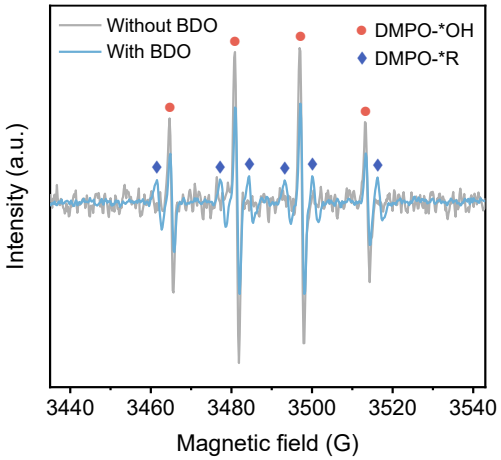

Fig. S19. The quasi-in-situ EPR spectra of $NiCo_2O_4$ electrocatalysts recorded at 1.5 V vs. RHE with and without BDO.

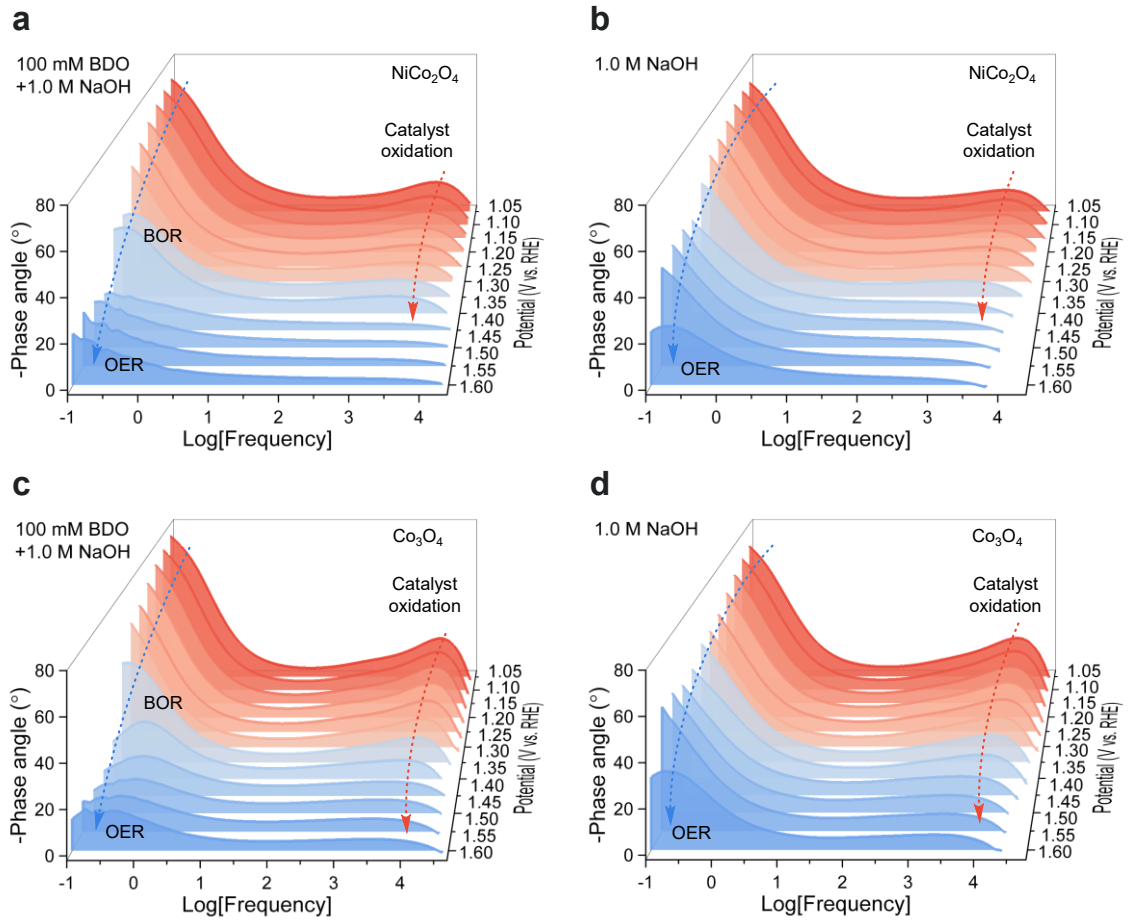

Fig. S20. Bode phase plots of the operando EIS on (a, b) $NiCo_2O_4$ electrocatalyst and (c, d) Co_3O_4 electrocatalyst in 1.0 M NaOH electrolyte with or without 0.1 M BDO.

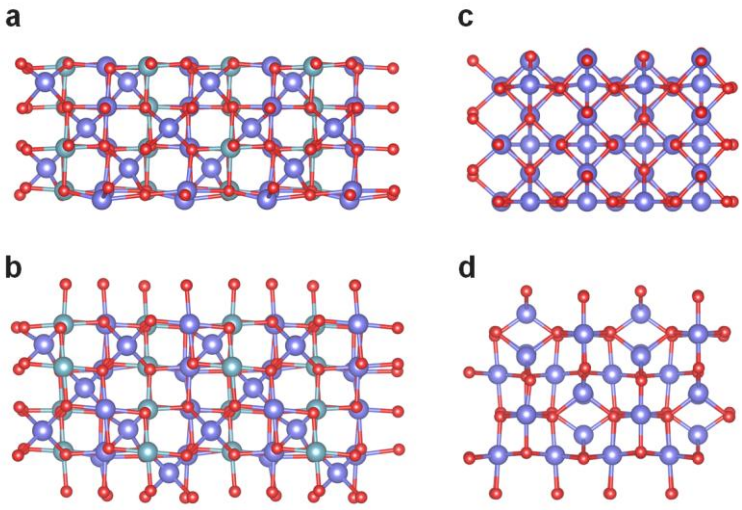

Fig. S21. The theoretical calculation models of $NiCo_2O_4$ with (a) side view and (b) top view, and Co_3O_4 (c) side view and (d) top view. Co, Ni and O atoms are depicted here as purple, green and red spheres, respectively.

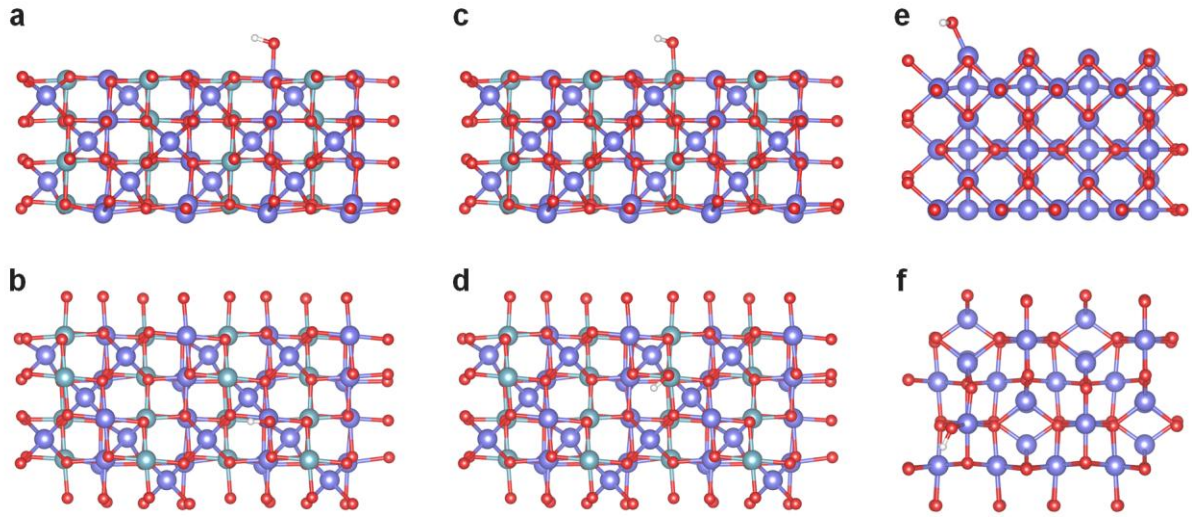

Fig. S22. The adsorption configurations of *OH on (a, b) Co site in $NiCo_2O_4$, (c, d) Ni site in $NiCo_2O_4$ and (e, f) Co site in Co_3O_4. Co, Ni, O and H atoms are depicted here as purple, green, red and white spheres, respectively.

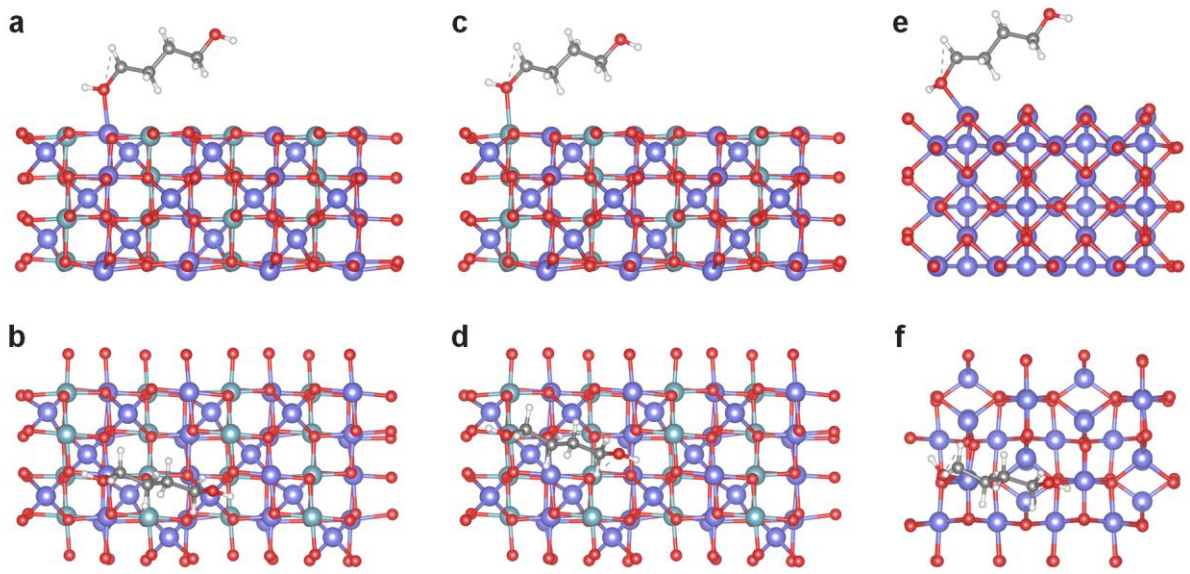

Fig. S23. The adsorption configurations of BDO on (a, b) Co site in $NiCo_2O_4$, (c, d) Ni site in $NiCo_2O_4$ and (e, f) Co site in Co_3O_4. Co, Ni, C, O and H atoms are depicted here as purple, green, gray, red and white spheres, respectively.

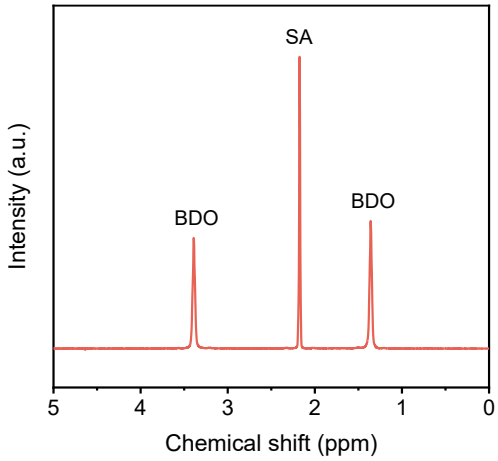

Fig. S24. ^{1}H NMR of the PBS hydrolysate solution.

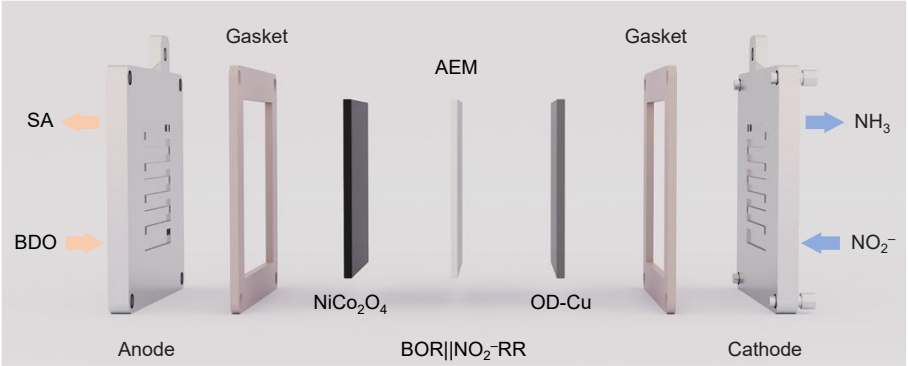

Fig. S25. Schematic diagram of MEA device for the paired BOR||NO_2^-RR system.

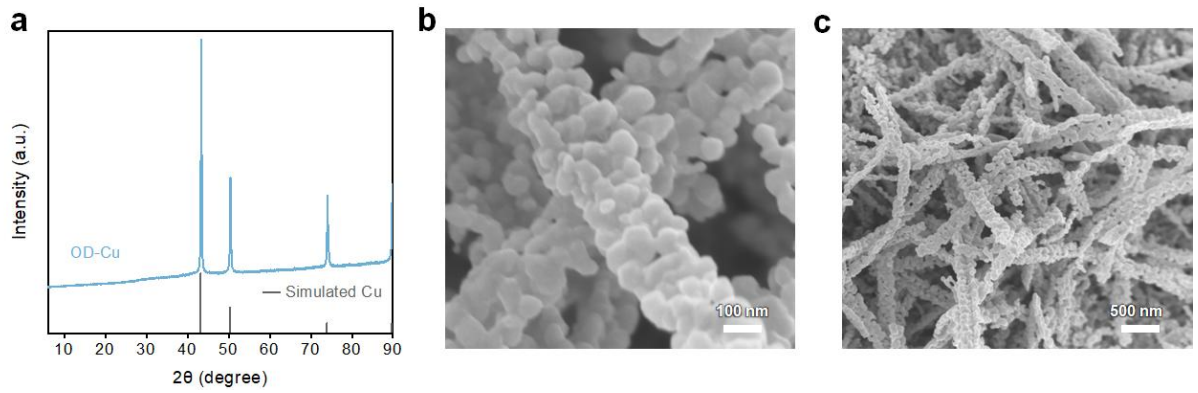

Fig. S26. (a) XRD pattern, (b-c) SEM images of OD-Cu electrocatalyst.

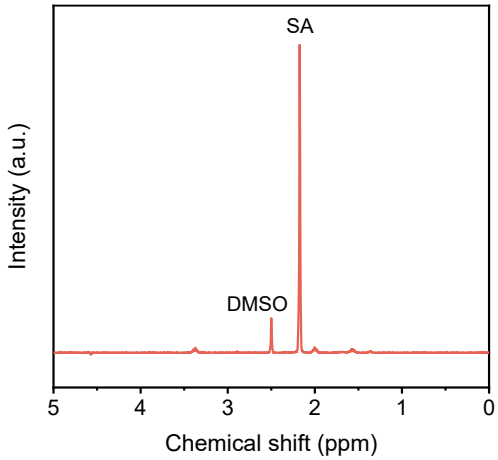

Fig. S27. ^{1}H NMR of the anolyte after electrocatalytic PBS hydrolysate upcycling in the MEA electrolyzer.

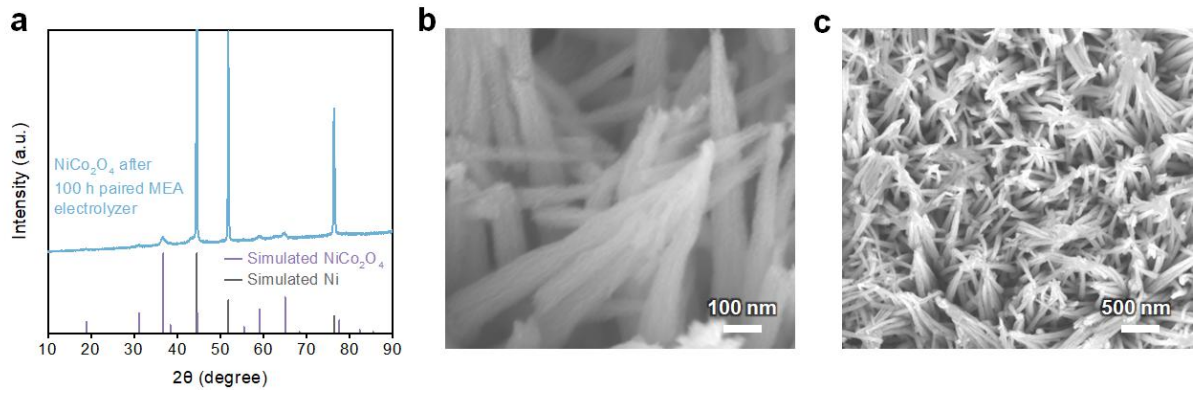

Fig. S28. (a) XRD pattern, (b-c) SEM images of the $NiCo_2O_4$ anode after electrochemical upgrading of PBS hydrolysate and NO_x in the MEA electrolyzer at 400 mA cm^{-2} for 100 hours.

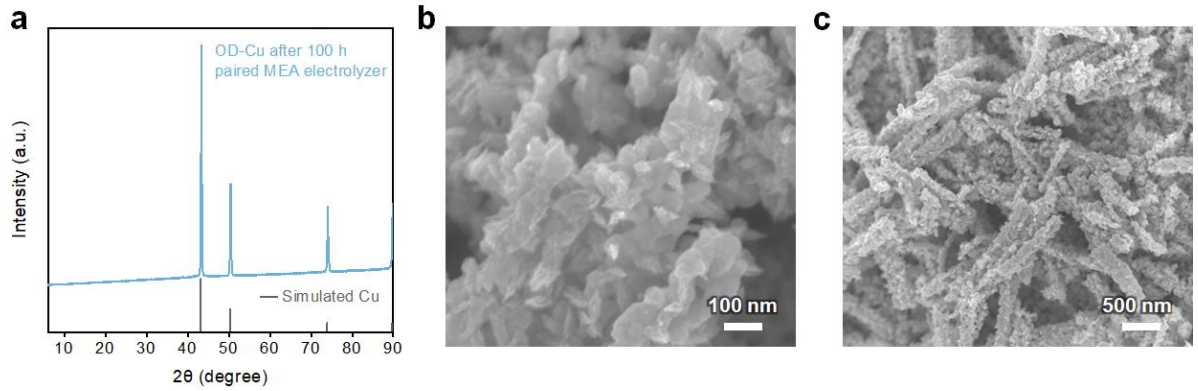

Fig. S29. (a) XRD pattern, (b-c) SEM images of OD-Cu cathode after electrochemical upgrading of PBS hydrolysate and NO_x in the MEA electrolyzer at 400 mA cm^{-2} for 100 hours.

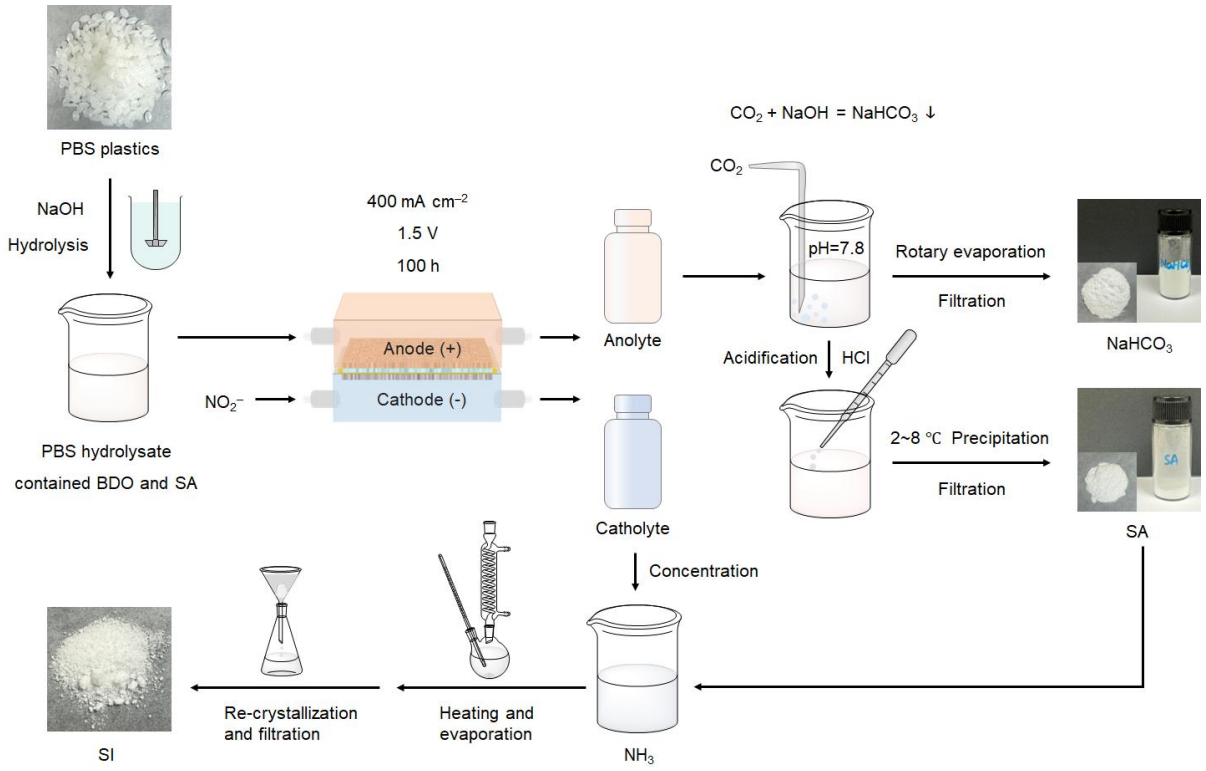

Fig. S30. Schematic illustrations and photographs of the full process for electrocatalytic upcycling of PBS plastics, CO_2-assisted sequential precipitation of $NaHCO_3$ and SA, as well as amination of SA to yield SI.

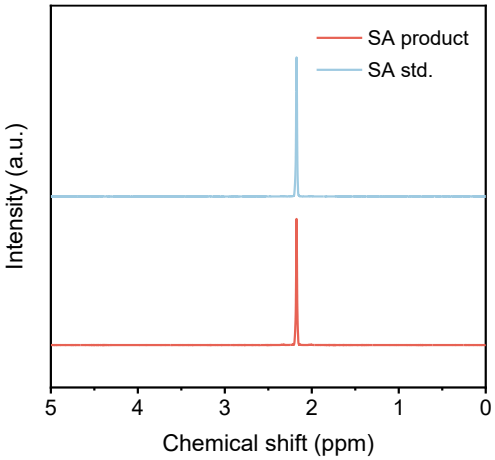

Fig. S31. ^{1}H NMR spectra of the SA product and standard.

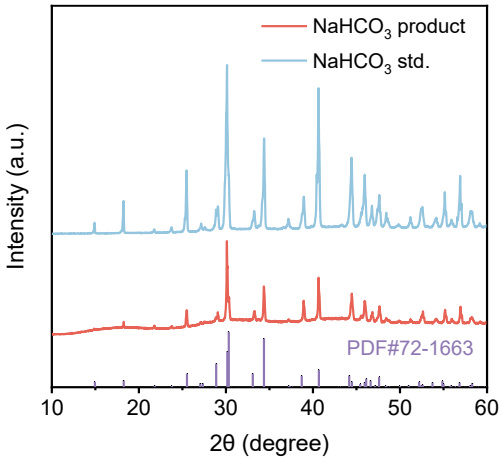

Fig. S32. XRD pattern of the $NaHCO_3$ product and standard.

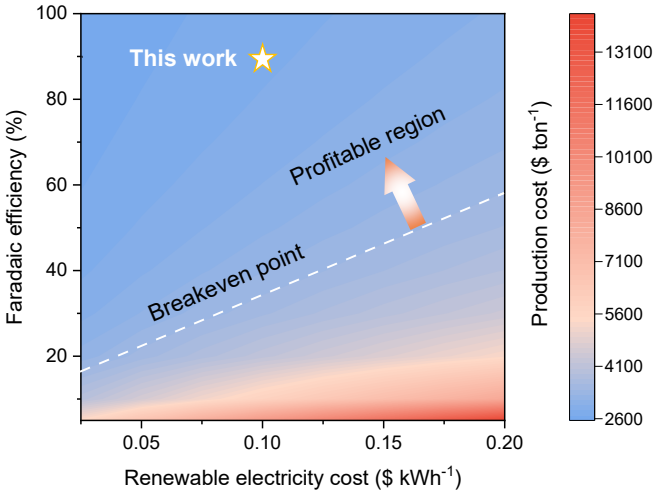

Fig. S33. The impact of Faradaic efficiency and renewable electricity cost on the production cost of the paired electro-upgrading of PBS plastics and NO_x.

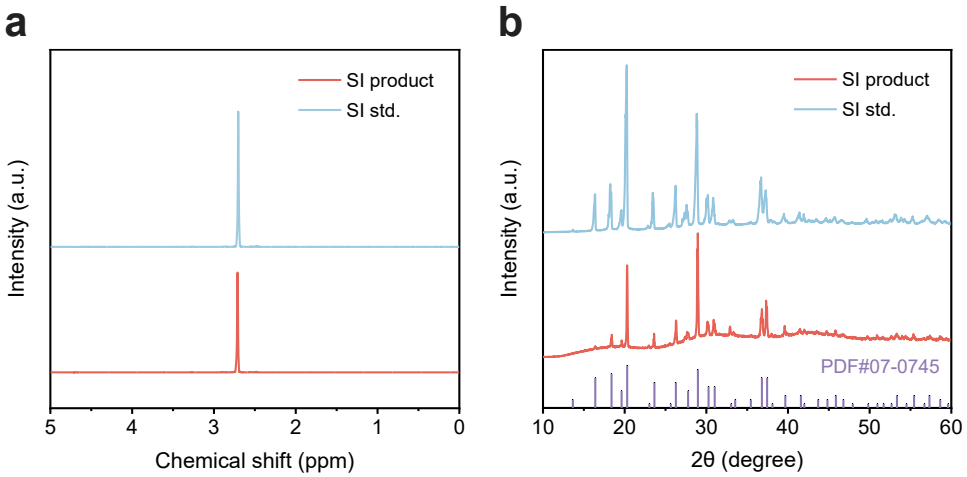

Fig. S34. (a) ^{1}H NMR spectra and (b) XRD pattern of the succinimide product and standard.

Table S1. Fitting parameters of Ni 2*p* XPS spectra for $NiCo_2O_4$ and NiO electrocatalyst.

Catalysts	Fitting of Ni 2*p*	Position (eV)	FWHM	Area
$NiCo_2O_4$	Ni^{2+} $2p_{3/2}$	854.01	1.40	6012.80
	Ni^{2+} $2p_{1/2}$	871.54	1.40	3006.40
	Ni^{3+} $2p_{3/2}$	855.64	3.03	20912.54
	Ni^{3+} $2p_{1/2}$	873.20	3.03	10456.27
NiO	Ni^{2+} $2p_{3/2}$	853.95	1.35	23598.93
	Ni^{2+} $2p_{1/2}$	871.32	1.35	11799.47
	Ni^{3+} $2p_{3/2}$	855.73	2.89	56357.71
	Ni^{3+} $2p_{1/2}$	873.08	2.89	28178.86

Table S2. Fitting parameters of Co 2*p* XPS spectra for $NiCo_2O_4$ and Co_3O_4 electrocatalyst.

Catalysts	Fitting of Co 2*p*	Position (eV)	FWHM	Area	Co^{2+}/Co^{3+}
$NiCo_2O_4$	Co^{3+} $2p_{3/2}$	779.43	1.88	12418.24	1.48
	Co^{3+} $2p_{1/2}$	794.55	1.88	6209.12	
	Co^{2+} $2p_{3/2}$	781.06	3.18	18382.58	
	Co^{2+} $2p_{1/2}$	796.45	3.18	9191.29	
Co_3O_4	Co^{3+} $2p_{3/2}$	779.68	1.84	18759.23	1.41
	Co^{3+} $2p_{1/2}$	794.77	1.84	9379.62	
	Co^{2+} $2p_{3/2}$	781.30	3.04	26506.82	
	Co^{2+} $2p_{1/2}$	796.61	3.04	13253.41	

Table S3. Fitting parameters of O 1*s* XPS spectra for $NiCo_2O_4$, Co_3O_4 and NiO electrocatalyst.

Catalysts	Fitting of O 1*s*	Position (eV)	FWHM	Area	O_b/O_a
$NiCo_2O_4$	O_a	529.42	1.24	14985.12	0.71
	O_b	530.98	1.92	10682.92	
	O_c	532.73	2.59	5373.99	
Co_3O_4	O_a	529.67	1.19	16207.38	0.39
	O_b	531.03	1.69	6273.58	
	O_c	531.93	3.25	6195.34	
NiO	O_a	529.49	1.22	21906.67	0.50
	O_b	531.18	1.45	10866.34	
	O_c	-	-	-	

Table S4. Comparison of anodic oxidation of BDO to SA using $NiCo_2O_4$ and other reported catalysts.

Catalyst	Electrolyte	Potential @ *J*	FE (%)	Yield (%)	Stability	Ref.
$NiCo_2O_4$	**1 M NaOH with 0.1 M BDO**	**1.50 V vs. RHE @ ~400 mA cm^{-2}**	**96.0**	**95.4**	**100 h**	**This work**
Cr^{3+}-$Ni(OH)_2$ /NF	1 M KOH with 0.05 M BDO	1.5 V vs. RHE @ ~150 mA cm^{-2}	93.0	95.9	14 h	[3]
Mo_1-CoSe-V_{Mo}/NF	1 M KOH with 0.1 M BDO	1.4 V vs. RHE @ ~400 mA cm^{-2}	94.0	~95.7	170 h	[4]
Mn_d-NiNDA	1 M KOH with 0.1 M BDO	1.35 V vs. RHE @ ~400 mA cm^{-2}	95.8	96.9	~21 h	[5]
NiBDC@$NiS_{0.68}$	1 M KOH with 0.1 M BDO	1.5 V vs. RHE	95.7	92.5	~24 h	[6]
T-NF	1 M KOH with 0.1 M BDO	1.36 V vs. RHE @50 mA cm^{-2}	93	-	20 h	[7]
Ni BDC-ACT	1 M KOH with 0.05 M BDO	1.57 V vs. RHE	>90	-	-	[8]

Table S5. The prices of input chemicals and products, taken from the relevant references[3, 6, 12-13] and online trading platforms (https://www.made-in-china.com/).

Chemicals	Price ($/ton)
PBS	390
NaOH	422
H_2O	0.22
$NaNO_2$	571
HCl	12.7
Succinic acid (SA)	1957
$NaHCO_3$	350
NH_3	750

References

1. G. Kresse and D. Joubert, *Phys. Rev. B*, 1999, **59**, 1758-1775.
2. J. P. Perdew, K. Burke, M. Ernzerhof, *Phys. Rev. Lett.*, 1997, **78**, 1396.
3. B. Zhou, K. Shi, X. Teng, Z. Li, L. Chen and J. Shi, *Angew. Chem. Int. Ed.*, 2024, **63**, e202411502.
4. J. Qi, Y. Xia, X. Meng, J. Li, S. Yang, H. Zou, Y. Ma, Y. Zhang, Y. Du, L. Zhang, Z. Lin and J. Qiu, *Adv. Mater.*, 2025, **37**, e2419058.
5. D. Xiong, X. He, X. Liu, K. Zhang, Z. Tu, J. Wang, S. G. Sun and Z. Chen, *ACS Nano*, 2024, **18**, 20340−20352.
6. D. Xiong, X. He, Z. Zhu, T. Liu, D. Wu, Y. Zou and Z. Chen, *Adv. Funct. Mater.*, 2026, **36**, e18434.
7. X. Liu, J. Wang, Z. Fang, S. Gong, D. Xiong, W. Chen, D. Wu and Z. Chen, *App. Catal. B: Environ.*, 2023, **334**, 122870.
8. Y. Zou, Q. Ren, T. Xia, J. Yang, C. Qi, Z. Li and M. Shao, *Small*, 2026, **22**, e14220.
9. P. De Luna, C. Hahn, D. Higgins, S. A. Jaffer, T. F. Jaramillo, E. H. Sargent, *Science*, 2019, **364**, 1-9.
10. B.-H. Zhao, F. Chen, M. Wang, C. Cheng, Y. Wu, C. Liu, Y. Yu, B. Zhang, *Nat. Sustain.*, 2023, **6**, 827837.
11. H. Zhou, Y. Ren, Z. Li, M. Xu, Y. Wang, R. Ge, X. Kong, L. Zheng, H. Duan, *Nat. Commun.*, 2021, **12**, 4679.
12. J. Li, X. Liu, S.-M. Xu, M. Xu, Y. Wang, Y. Lyu, A.-Z. Li, Y. Wang, X. Wang, T. Zhou, H. Zhou, Y. Peng, X. Li, L. Zheng and H. Duan, *Nat. Synth.*, 2025, **4**, 1598–1609.
13. H. Wang, B. Yang, R. L. Smith Jr., Y. Su, X. Qi, *Adv. Funct. Mater.*, 2025, **35**, 2425333.